Volume 12 | Number 8 | 21 April 2025

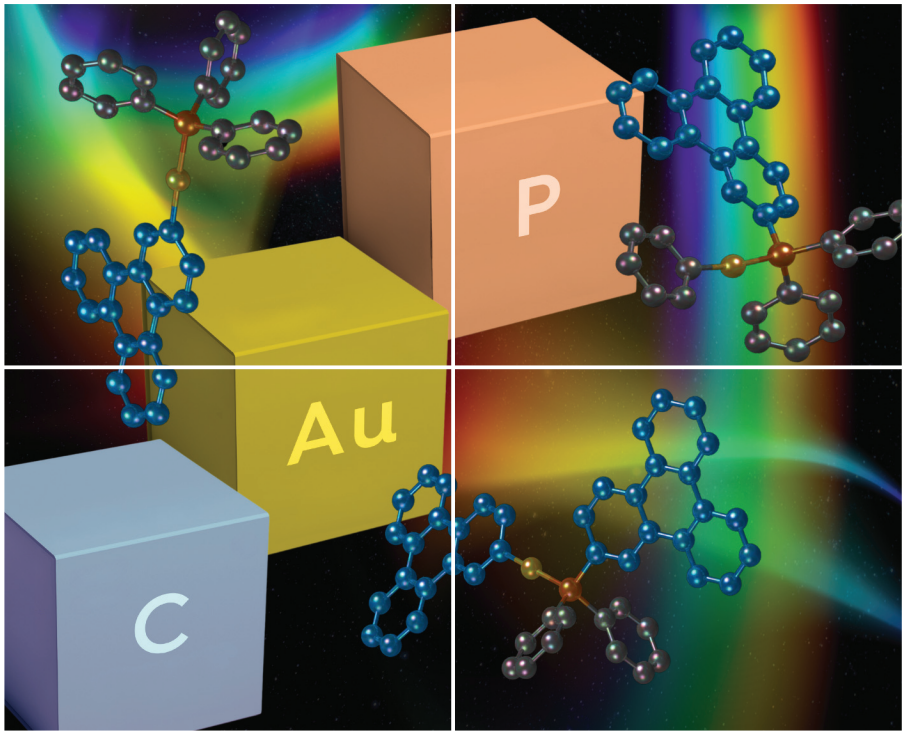

INORGANIC CHEMISTRY FRONTIERS

CCS 中国化学会 CHINESE CHEMICAL SOCIETY
PEKING UNIVERSITY 1898
ROYAL SOCIETY OF CHEMISTRY
rsc.li/frontiers-inorganic

INORGANIC CHEMISTRY FRONTIERS

RESEARCH ARTICLE

View Article Online
View Journal | View Issue

Open Access Article. Published on 22 January 2025. Downloaded on 1/19/2026 5:16:09 PM.
This article is licensed under a Creative Commons Attribution-NonCommercial 3.0 Unported Licence.

Check for updates

Cite this: *Inorg. Chem. Front.*, 2025, **12**, 3041

Tuning luminescence in gold(I)-phosphine complexes: structural, photophysical, and theoretical insights†

Anyie P. Atencio,[a] Sergi Burguera,[b] George Zhuchkov,[a] Araceli de Aquino,[a] Jas S. Ward,[c] Kari Rissanen,[c] João Carlos Lima,[d] Inmaculada Angurell,[a] Antonio Frontera[b] and Laura Rodríguez *[a]

Received 16th December 2024,
Accepted 20th January 2025

DOI: 10.1039/d4qi03225j

rsc.li/frontiers-inorganic

Gold(I) complexes featuring phosphine ligands functionalized with chromophores such as triphenylene, phenanthrene, and carbazole were synthesized and systematically studied to explore the relationship between molecular structure and luminescence properties. Comprehensive photophysical characterization revealed that the coordination environment and chromophore positioning significantly influence intersystem crossing, phosphorescence, and aggregation behavior. In solution, aggregation-induced phenomena were probed using computational tools, including density functional theory (DFT) and non-covalent interaction (NCI) analysis, revealing diverse π-stacking and Au···π interactions. Distinct photophysical trends were identified among the three series of compounds, with triphenylene derivatives exhibiting aggregation-induced emission broadening and phenanthrene derivatives showing strong heavy atom effects. The combination of experimental and theoretical insights provides a foundation for designing luminescent materials with tunable properties for optoelectronic applications.

Introduction

Gold(I) complexes have been extensively studied for their unique luminescent properties, which arise from various electronic transitions including metal-centered transitions and ligand-to-metal charge transfer (LMCT). They are frequently affected by the presence of metal···metal contacts, usually known as aurophilic interactions. These photophysical properties make gold(I) complexes attractive candidates for applications in optoelectronic devices, sensors, and bioimaging, among others.[1–12] Traditionally, phosphine ligands have been widely employed in the coordination sphere of gold(I) complexes due to their strong σ-donating abilities. However, the luminescence of such complexes typically arises from other ligands coordinated to the metal center, with phosphine playing a more structural or electronic role rather than contributing to the emissive properties.[13–18]

Recent advances in ligand design have demonstrated that phosphine ligands can be functionalized with chromophores to exhibit intrinsic luminescent properties.[19–25] Phosphines containing extended aromatic chromophores have been shown to display intrinsic fluorescence due to their extended π-conjugation and favorable photophysical characteristics, including high quantum yields and photostability.[26–30] These functionalized phosphine introduce a novel approach to luminescent gold(I) complexes, where the phosphine itself can participate in or enhance the overall emission and self-assembling processes.

This study focuses on the synthesis and photophysical characterization of gold(I) complexes containing luminescent phosphine ligands, where the chromophore is either positioned on the phosphine ligand, on a second coordination ligand, or on both. This will have direct applications in tuning the emissive properties of these metal complexes and will provide foundational insights into how luminescence can be tuned in materials more generally.

The impact of the chromophore's location on the photophysical behavior of the gold(I) complexes is herein systematically explored, with a particular emphasis on intersystem crossing (ISC), and the influence of intermolecular weak interactions such as π–π stacking and aurophilicity.[8,22]

[a]*Departament de Química Inorgànica i Orgànica, Secció de Química Inorgànica, Universitat de Barcelona and Institut de Nanociència i Nanotecnologia (IN2UB), Martí i Franquès 1-11, E-08028 Barcelona, Spain. E-mail: laurarodriguezr@ub.edu*
[b]*Departament de Química, Universitat de les Illes Balears, 07122 Palma de Mallorca, Spain*
[c]*University of Jyvaskyla, Department of Chemistry, 40014 Jyväskylä, Finland*
[d]*LAQV-REQUIMTE, Departamento de Química, Faculdade de Ciências e Tecnologia, Universidade Nova de Lisboa, 2829-516 Caparica, Portugal*

† Electronic supplementary information (ESI) available. CCDC 2409503–2409506. For ESI and crystallographic data in CIF or other electronic format see DOI: https://doi.org/10.1039/d4qi03225j

Open Access Article. Published on 22 January 2025. Downloaded on 1/19/2026 5:16:09 PM.
This article is licensed under a Creative Commons Attribution-NonCommercial 3.0 Unported Licence.

Several gold(I) complexes featuring chromophore-functionalized phosphines were synthesized and characterized in this work, to evaluate the impact of the chromophore location on their structural and photophysical properties. In addition, density functional theory (DFT) calculations were performed to provide insights into the electronic structure, intersystem crossing mechanisms, and aggregation in solution. By integrating experimental and theoretical approaches, this study aims to establish structure–property relationships that can guide the design of novel luminescent materials for advanced applications in optoelectronics and sensing.

Results and discussion

Synthesis and characterization

Three series of gold(I) compounds which differ in the type of chromophore and the position of coordination of the gold(I) atom have been synthesized following the procedure displayed in Scheme 1. Three series of compounds have been synthesized that have been named as series 1 (those containing triphenylene, Triphen, as ligand), series 2 (those containing phenanthrene, Phen, as ligand) and series 3 (those containing carbazole, Cz). It requires the previous preparation of different

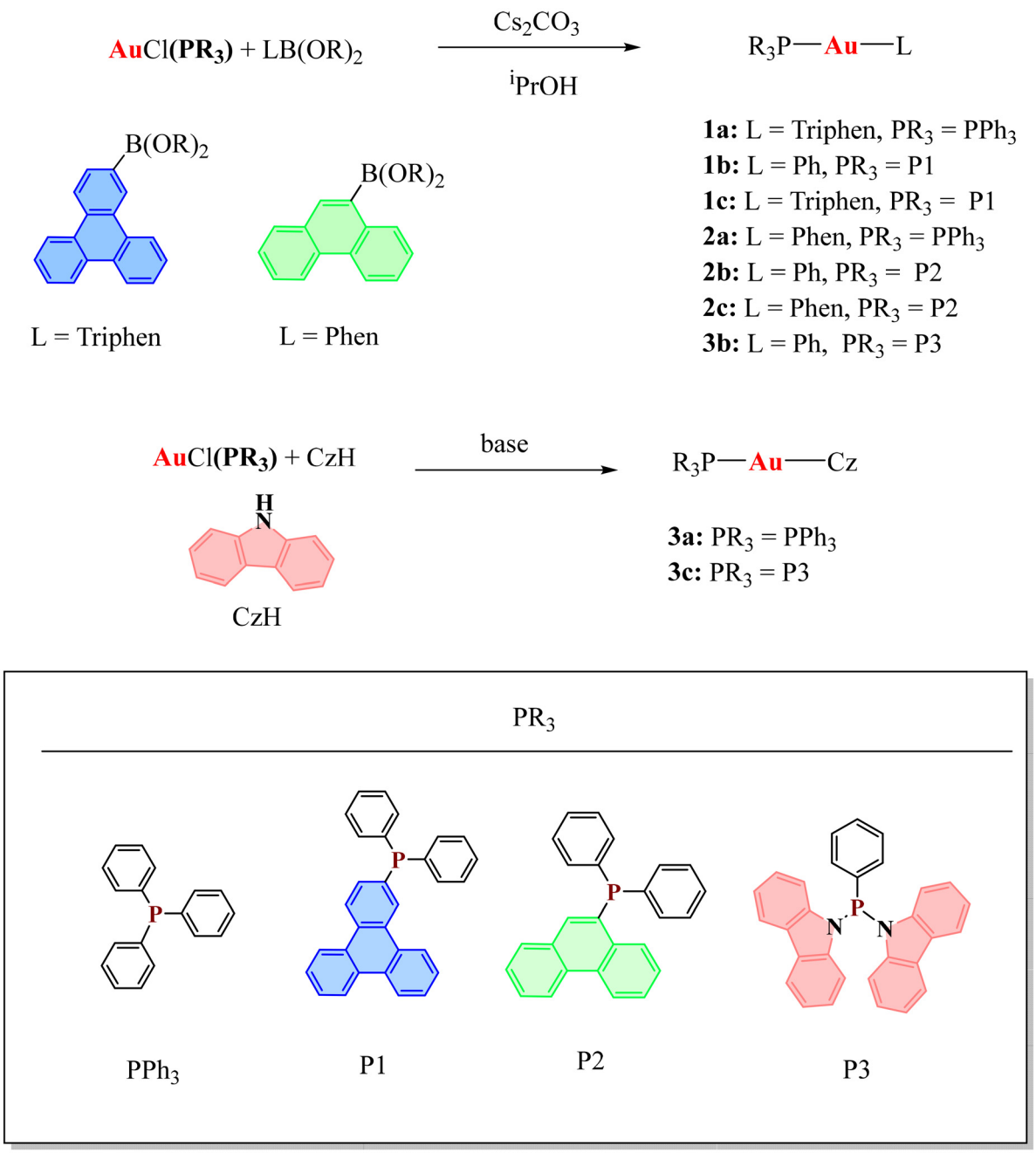

Scheme 1 Synthetic procedure of the phosphine gold(I) complexes. Reaction conditions: **1a**, **2a**, **1b**, **2b**, **3b**, **1c**, and **2c**: 5 days reaction at RT; **3a**: KOH, 1 h in MeOH and **3c**: K_2CO_3, 24 h reaction in $CH_3(CO)CH_3$ at RT.

Open Access Article. Published on 22 January 2025. Downloaded on 1/19/2026 5:16:09 PM.
This article is licensed under a Creative Commons Attribution-NonCommercial 3.0 Unported Licence.

phosphine ligands (PR_3) according to the reported procedure[21,31] for the lithiation of the corresponding aromatic halide followed by the addition of the chlorophosphane (see Scheme S1†). After chromatographic purification, the desired ligands **P1** containing triphenylene (Triphen), **P2**, with phenanthrene (Phen), and **P3**, with carbazole (Cz), were obtained as white powders. Subsequently, the [AuCl(PR_3)] precursors were obtained in good yields by simple reaction with a stoichiometric amount of [AuCl(tht)] (tht = tetrahydrothiophene), as the gold(I) source, and the corresponding phosphine (Scheme S1†). The correct formation of the compounds was evidenced in the $^{31}P\{^1H\}$ NMR spectra where the phosphorus signal showed a downfield shift (20–30 ppm) with respect to the corresponding free phosphine.

The [AuCl(PR_3)] compounds were used as precursors to synthesize a wide variety of gold(I) compounds that differ on: (1) having the chromophore linked directly to the Au(I) metal centre (**1–3a**); (2) having a chromophore at the phosphine unit (**1–3b**); (3) having the chromophore in both coordination positions (**1–3c**), opening a wide variety of exhibiting possibilities in the field of luminescent gold(I) compounds. In particular, we aim at exploring the effect of the heavy atom effect on the T_1 population of the chromophores depending on their structural coordination position.

These gold(I) complexes were synthesized with slight modification of a previously reported method (see Scheme 1).[32–35]

In the case of series **1**, **2**, and **3b**, a solution of the organoboronic acid or the pinacol ester and the corresponding [AuCl(PR_3)] precursor in the presence of excess caesium carbonate as a base was maintained under stirring in isopropanol at RT for 5 days under inert atmosphere. Then the solvent was evaporated, and the final product was extracted with dichloromethane. In the case of complexes **3a** and **3c** a carbazole solution and the [AuCl(PR_3)] were stirred in the presence of a base.

The compounds were characterized by ^1H, $^{31}P\{^1H\}$ and $^{13}C\{^1H\}$ NMR, as well as by 2D ^1H–^1H COSY and ^1H–^{13}C HSQC NMR and IR spectroscopy techniques and mass spectrometry (see Fig. S1–S53†). The ^1H NMR spectra show the signals of both the chromophore and phosphine moieties with the expected integration. As expected by the chemical equivalence of the phosphorus atoms, the $^{31}P\{^1H\}$ NMR spectra show only one signal whose chemical shift appears slightly downfield shifted (5–10 ppm) with respect to that of the [AuCl(PR_3)] precursor, which is an indication of the successful formation of pure products.

Single crystals suitable for X-ray diffraction analysis were successfully grown for **1a**, **1b**, **3a**, and **3b** from slow diffusion of hexane into dichloromethane solutions of the complexes at room temperature. The corresponding molecular structures are presented in Fig. 1 and the selected bond lengths and angles are summarized in Table 1. Linear coordination of ligands at the Au(I) centers is observed, with P–Au–C angles of 177.6°(1), 172.5°(1) and 178.8°(7) for **1a**, **1b** and **3b**, respectively and 171.9°(2) for **3a**. No aurophilic contacts are observed in any of the structures (Fig. 2).

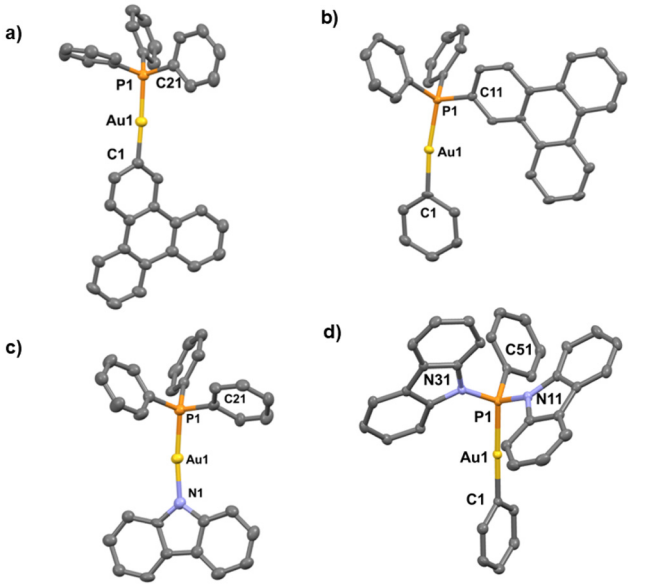

Fig. 1 X-ray crystal structures of **1a** (a) **1b** (b), **3a** (c), and **3b** (d). Yellow: gold; orange: phosphorus; blue: nitrogen and grey: carbon. All hydrogens have been omitted for clarity.

Table 1 Selected bond lengths (Å) and angles (°) for **1a**, **1b**, **3a**, and **3b**

1a			
Distance	(Å)	Angle	(°)
Au(1)–C(1)	2.054(3)	C(1)–Au(1)–P(1)	177.6(1)
Au(1)–P(1)	2.297(9)	Au(1)–P(1)–C(21)	112.6(1)
P(1)–C(21)	1.816(4)		
1b			
Distance	**(Å)**	**Angle**	**(°)**
Au(1)–C(1)	2.058(4)	C(1)–Au(1)–P(1)	172.5(1)
Au(1)–P(1)	2.299(1)	Au(1)–P(1)–C(11)	110.3(1)
P(1)–C(11)	1.816(4)		
3a			
Distance	**(Å)**	**Angle**	**(°)**
Au(1)–N(1)	2.018(7)	N(1)–Au(1)–-P(1)	171.9(2)
Au(1)–P(1)	2.236(2)	Au(1)–P(1)–C(21)	107.0(3)
P(1)–C(21)	1.800(1)		
3b			
Distance	**(Å)**	**Angle**	**(°)**
Au(1)–C(1)	2.046(3)	C(1)–Au(1)–P(1)	178.8(7)
Au(1)–P(1)	2.286(7)	Au(1)–P(1)–N(11)	111.78(7)
P(1)–N(11)	1.707(2)	Au(1)–P(1)–N(31)	114.84(8)
P(1)–N(31)	1.701(2)		
P(1)–C(51)	1.790(3)		

The 3D packing of complexes displays a conformation driven by the establishment of C–H···π interactions between a π ring of the chromophore and the phosphine moieties (**2a**,[36] **3a**, and **3b**) or between different phosphine moieties (**1a** and **1b**). Moreover, the packing of **1b** shows the superposition of the triphenylene in a staggered conformation and causes π–π stacking (distances of 3.115 Å for **1b** and 4.759 Å for **3b**). When comparing the dimers in series 1, it is observed that the chromophore, when linked to the phosphine moiety, is capable of stacking and forming π–π interactions. In contrast,

Open Access Article. Published on 22 January 2025. Downloaded on 1/19/2026 5:16:09 PM.
This article is licensed under a Creative Commons Attribution-NonCommercial 3.0 Unported Licence.

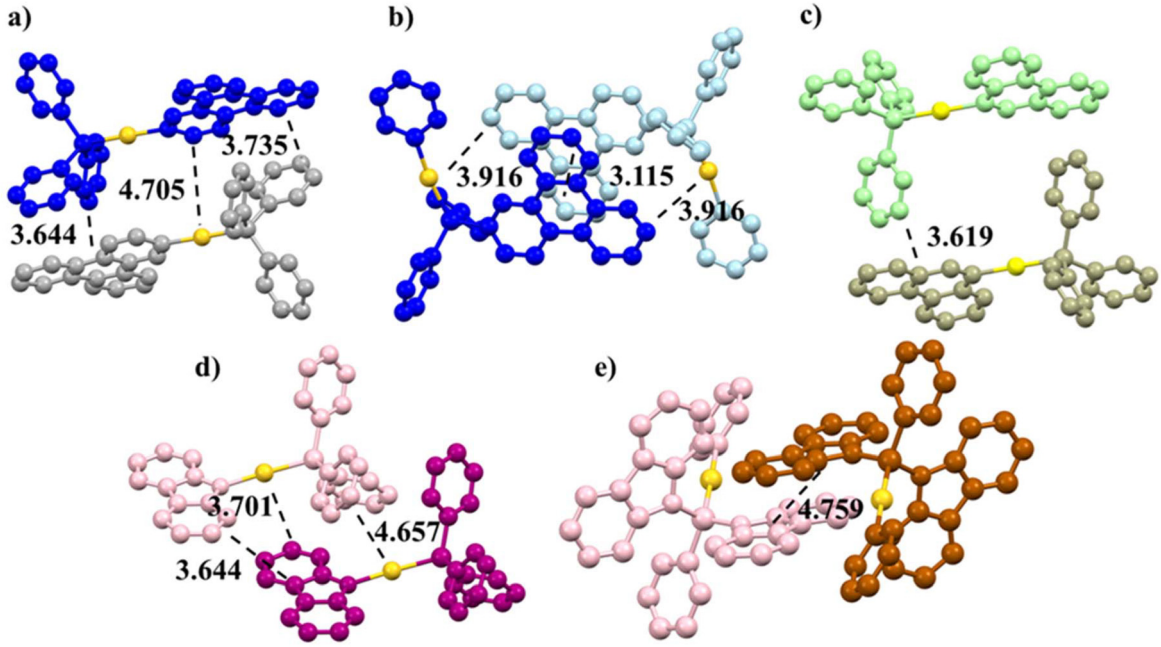

Fig. 2 3D crystal packing of complex **1a** (a), **1b** (b), **2a** (c), **3a** (d) and **3b** (e). The crystal structure of **2a** was published previously by us in ref. 36 and has been included for comparison purposes.

when the chromophore is directly attached to the Au(I) center, π–π stacking is not observed. In series 3, however, π–π interactions are present in both scenarios: when the gold atom is bound to the chromophore and when it is bound to a phenyl group. This indicates that, regardless of the structural configuration around the gold atom, the carbazole unit retains its ability to establish π–π interactions (Fig. 2 and S54–S58–S52†).

Photophysical characterization

Absorption and emission spectra were recorded in 1×10^{-5} M dichloromethane solutions for the three series of complexes and the results are summarized in Table 2. The absorption spectra of all compounds exhibit typical bands in the 230–310 nm range due to π–π* intra-ligand transitions corresponding to the different chromophores (see Fig. S59†).[20,36,37] The shape and position of these bands for the gold(I) complexes and their free phosphine ligands **P1–P3** are very similar in all cases. The TD-DFT calculations performed at the CAM-B3LYP(dcm)/def2-TZVP//RI-BP86-D4/def2-TZVP level of theory for the three series of compounds demonstrate a reasonable agreement between the observed and calculated absorption bands (see Table 2). As an example, the computed spectrum of compound **1a** is shown overlapped with the experimental spectrum in Fig. 3. Both spectra exhibit a similar band structure, with the calculated bands consistently blue-shifted by 20–30 nm relative to the experimental ones.

The lowest-energy transition band comprises two excitations ($S_0 \rightarrow S_1$ and $S_0 \rightarrow S_2$), with the natural transition orbitals (NTOs) depicted in Fig. 3b. These NTOs reveal that the transitions correspond to a π → π* charge transfer. The next observable band, associated with the $S_0 \rightarrow S_5$ excitation, displays a mixed intra-ligand charge transfer (ILCT) and ligand-to-metal charge transfer (LMCT) character.

The possibility of aggregation of the compounds in solution has been analyzed for selected examples. Given the richness in aromatic rings and the variety of possible conformations and aggregation modes, we focused on the structures depicted in Fig. 1. Initially, aggregation in the solid state was analyzed to identify potential dimeric assemblies. The most stable dimer from the solid-state analysis was selected as a starting point for optimization in solution using a continuum model with dichloromethane (DCM) as the solvent. Frequency calculations were performed to confirm the minimum-energy nature of the assemblies and to compute the free energies of complexation relative to the isolated monomers. Additionally, the noncovalent interactions contributing to dimer formation were visualized in real space using noncovalent interaction plots (NCIplot), as shown in Fig. 4.

The results reveal that centrosymmetric dimers are formed in compounds where the Au atom is bonded to a phenyl group (**1b** and **3b**) or phenanthrene group (**2a**). These dimers are stabilized by a combination of π-stacking interactions between the aromatic rings of the triphenylene, phenanthrene and carbazole chromophores and CH···π interactions involving the C–H bonds of these chromophores and the π-system of either the phenyl ring (in **1b**) or the carbazole (Cz) ring (in **3b**). In case of **2a**, the C–H···π contacts are established between tha H-atoms of the phenyl ring and the phenanthrene's π-system. These interactions are clearly visible as large green reduced density gradient (RDG) isosurfaces in the NCIplot. In contrast, when the triphenylene or carbazole chromophore is directly con-

Open Access Article. Published on 22 January 2025. Downloaded on 1/19/2026 5:16:09 PM.
This article is licensed under a Creative Commons Attribution-NonCommercial 3.0 Unported Licence.

Table 2 Absorption and emission data of the different series of the compounds in dichloromethane at 1×10^{-5} M and ratio of phosphorescence and fluorescence intensities, I_P/I_F, in N_2-sat solutions. Excitation energies associated transition and oscillator strength and Singlet–triplet (S_1–T_1) gap are given at the CAM-B3LYP(solvent = CH_2Cl_2)/def2-TZVP//RI-BP86-D4/def2-TZVP level of theory

Cmpnd	Absorption λ_{max}, nm ($\varepsilon \times 10^4$ M^{-1} cm^{-1})	Fluorescence emission air-equilibrated λ_{max} (nm)	Phosphorescence emission N_2-saturated λ_{max} (nm)	I_P/I_F RT (77 K)	Excitation Energy and oscillator strength	S_1–T_1 gap
P1	266 (8.35), 314 (1.54)	363	—	–(0.36)	—	
AuCl(**P1**)	271 (6.48), 314 (0.98)	371	462	2.2 (13.1)	—	
1a	272 (5.91), 309 (1.45)	381 (3.25 eV)	459 (2.70 eV)	14.1 (12.1)	$S_0 \rightarrow S_1$ 4.23 eV (293 nm) $f = 0.0030$	0.57 eV
1b	268 (1.77), 311 (3.77)	381 (3.25 eV)	460 (2.69 eV)	3.0 (19.7)	$S_0 \rightarrow S_1$ 4.22 eV (294 nm) $f = 0.0180$	0.46 eV
1c	267 (8.84), 314 (1.08)	372 (3.33 eV)	463 (2.68 eV)	0.9 (24.2)	$S_0 \rightarrow S_1$ 4.22 eV (294 nm) $f = 0.0085$	0.99 eV
P2	255 (5.73), 300 (92.7)	372	—	–(2.6)	—	
AuCl(**P2**)	261 (5.26), 309 (1.06)	374	496	0.9 (15.7)	—	
2a	255 (6.05), 313 (1.63)	368 (3.37 eV)	500 (2.48 eV)	7.5 (112.3)	$S_0 \rightarrow S_1$ 4.16 eV (298 nm) $f = 0.0109$	0.48 eV
2b	254 (9.05), 313 (2.12)	378 (3.28 eV)	501 (2.47 eV)	4.2 (29.8)	$S_0 \rightarrow S_1$ 4.20 eV (295 nm) $f = 0.0068$	0.39 eV
2c	261 (4.64), 308 (1.00)	372 (3.33 eV)	496 (2.50 eV)	1.3 (46.4)	$S_0 \rightarrow S_1$ 4.16 eV (298 nm) $f = 0.0115$	1.09 eV
P3	235 (8.13), 288 (2.30)	380	—	–(9.8)	—	
AuCl(**P3**)	231 (11.17), 288 (2.82)	371	—	–(10.5)	—	
3a	237 (6.77), 293 (1.36)	347 (3.57 eV)	—	–(43.8)	$S_0 \rightarrow S_2$ 4.23 eV (293 nm) $f = 0.1193$	0.99 eV
3b	233 (13.10), 291 (3.74)	347 (3.57 eV)	—	–(9.8)	$S_0 \rightarrow S_3$ 4.52 eV (274 nm) $f = 0.0397$	0.41 eV
3c	233 (8.92), 291 (3.73)	346 (3.58 eV)	—	–(4.6)	$S_0 \rightarrow S_3$ 4.36 eV (284 nm) $f = 0.1520$	1.23 eV

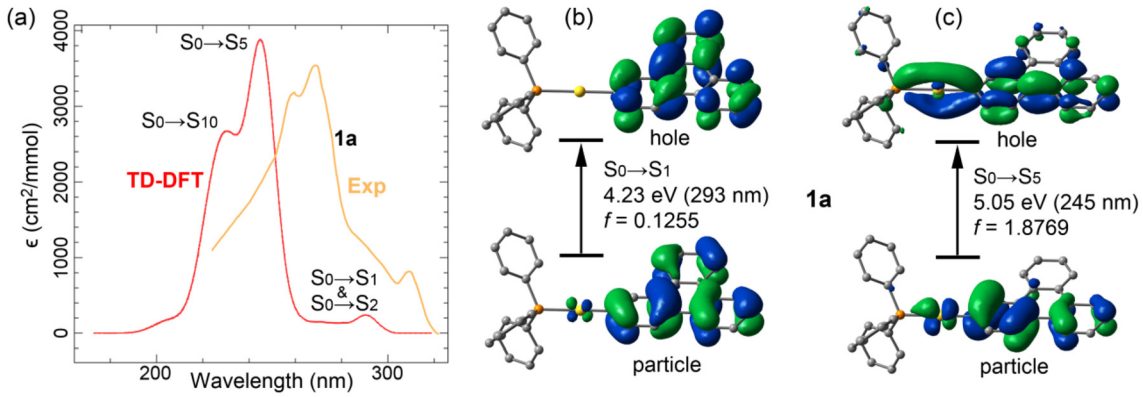

Fig. 3 (a) Experimental and theoretical UV-vis spectra of compound **1a** with indication of the main excitations responsible for the band. (b) NTOs corresponding to the lowest energy band. (c) NTOs corresponding to the $S_0 \rightarrow S_5$ excitation. The theoretical excitation energies and oscillator strengths are indicated.

nected to the Au center (as in **1a** and **3a**), the assemblies are more complex and exhibit less symmetric dimers.

The NCIplot for these compounds indicates that π-stacking interactions are still dominant, but additional forces, such as Au···π and Au···C interactions, also play a significant role in stabilizing the dimers. The free energy of formation of the dimers is highly negative in all cases, suggesting that these dimers are most likely present in solution, even at low concentrations. This highlights the significant role of noncovalent interactions, including π-stacking, CH···π, and metal-involved contacts, in driving the aggregation behavior of these compounds.

The significant broadening observed in the spectra of the triphenylene-based compounds (series 1, Fig. S59†) can be attributed to the formation of aggregates in solution. This behavior is likely due to the exposure and preorganization of the triphenylene units in the dimer, facilitating oligomer formation. In contrast, the geometries of the dimers in series 3 (Fig. 4c and d) suggest a lack of preorganization in solution, which may hinder the formation of extended aggregates. A similar lack of preorganization is observed in the optimized geometry of dimer **2a**, represented in Fig. 4c. These findings indicate that series 1 is inherently more predisposed to form

Open Access Article. Published on 22 January 2025. Downloaded on 1/19/2026 5:16:09 PM.
This article is licensed under a Creative Commons Attribution-NonCommercial 3.0 Unported Licence.

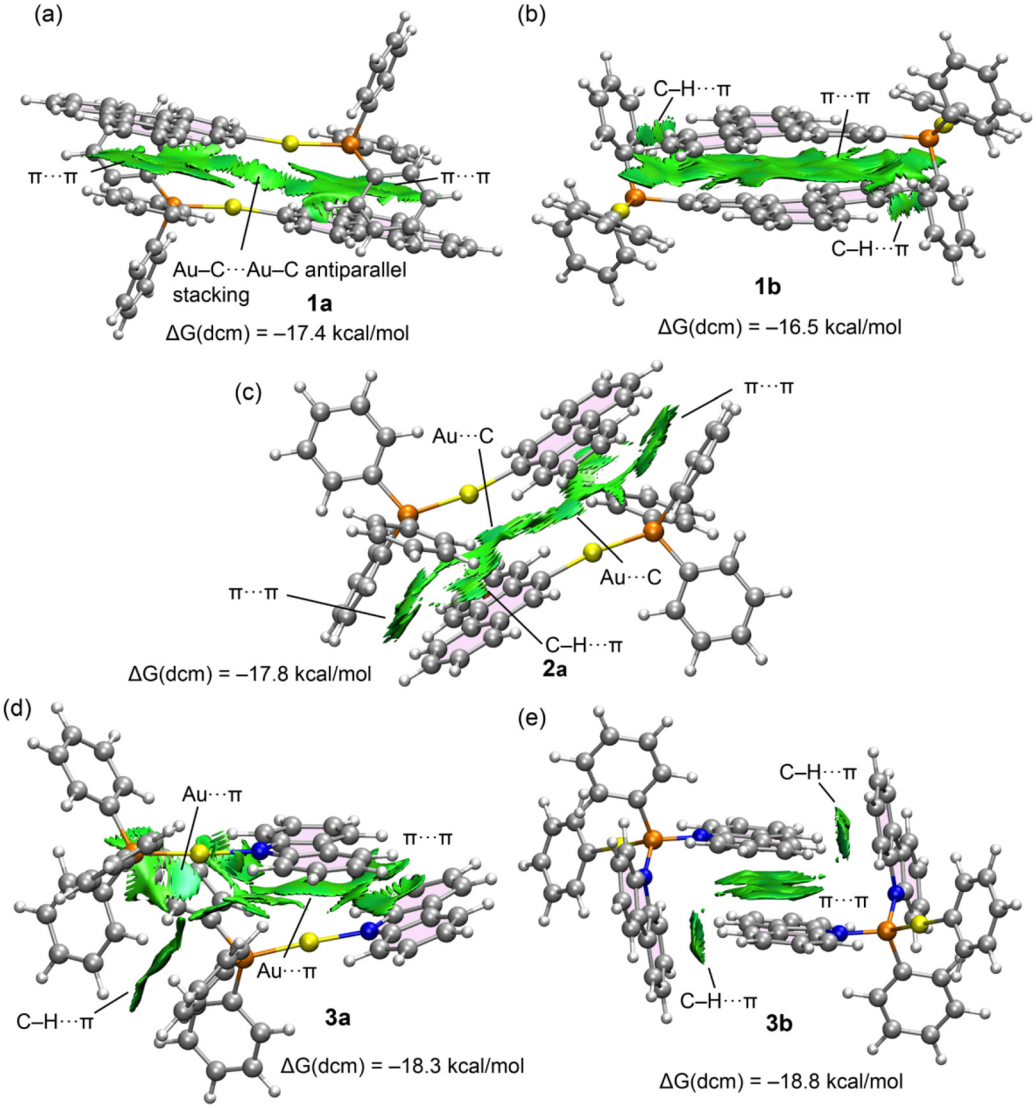

Fig. 4 Optimized geometries (RI-BP86-D4/def2-TZVP) of the dimers of **1a** (a), **1b** (b), **2a** (c), **3a** (d), and **3b** (e). Free Gibbs energies for the dimerization in dichoromethane are also indicated. The setting for the NCIplot representation are RDG = 0.5, ρ cut-off = 0.05, color scale -0.04 a.u. $\leq$ (sign λ_2)$\rho \leq -0.04$ a.u.

larger supramolecular assemblies, likely due to the structural alignment and interaction potential of the triphenylene core.

Emission spectra were recorded upon excitation the samples at the absorption maxima and at air-equilibrated and nitrogen saturated solution conditions (Fig. 5). All compounds display a vibronically structured emission band corresponding to the ^{1}IL emission of the chromophore.[38,39] A second broad emission band at *ca.* 520 nm is recorded for **P1**, ascribed to the corresponding triphenylene excimer.[40,41]

Several trends can be retrieved in all three series of compounds, both in air-equilibrated and N_2-saturated samples. The triphenylene (series 1) and phenanthrene (series 2) derivatives exhibit similar behavior, which is distinct from the carbazole compounds and will be discussed then separately. Regarding series 1 and 2, fluorescence emission bands can be observed for all compounds in air equilibrated conditions (including **P1** and **P2** and the [AuClPx] precursors), with the free phosphines **P1** and **P2** being those presenting higher fluorescence intensity (Fig. 5). The presence of the gold(I) heavy atom induces a significantly stronger reduction in fluorescence emission, that is associated to the increase in the population of the triplet excited state (see Table 2), as confirmed by the increase in ratio between phosphorescence and fluorescence (I_P/I_F).

Compounds **2a** and **2b** exhibit smaller S_1–T_1 gaps compared to compounds **1a**, **3a** and **1b**, **3b**, respectively. In the case of **2c**, the S_1–T_1 gap is smaller than that of **3c** but slightly larger than **1c**. This suggests that while the S_1–T_1 gap plays a key role, it is not the sole factor influencing emission behavior, since aggregation effects may also contribute significantly to the triplet to singlet population ratio. In fact, the HOMO–LUMO gap is reduced in the dimers (0.28–0.45 eV) in comparison

Open Access Article. Published on 22 January 2025. Downloaded on 1/19/2026 5:16:09 PM.
This article is licensed under a Creative Commons Attribution-NonCommercial 3.0 Unported Licence.

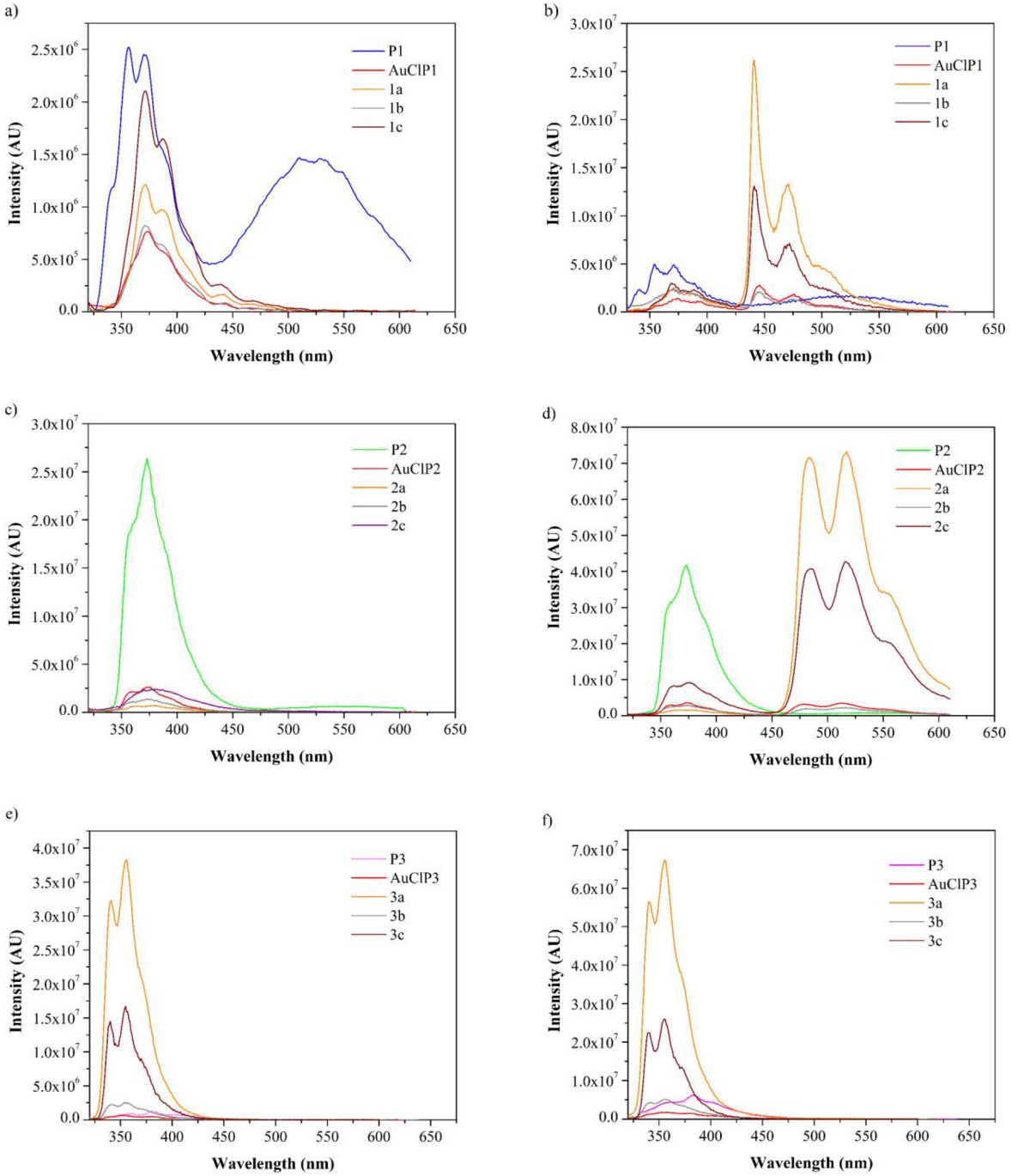

Fig. 5 Emission spectra of (a) series 1 air-equilibrated conditions; (b) series 1 N_2-saturated conditions; (c) series 2 air-equilibrated conditions; (d) series 2 N_2-saturated conditions (e) series 3 air-equilibrated conditions (f) series 3 N_2-saturated conditions of 1.0×10^{-5} M dichloromethane solutions, λ_{exc} = 310 nm.

with the monomers, see Table S5.† The fluorescence emission intensity of **3a–3c** follows the order **3a** > **3c** > **3b** both in air-equilibrated and N_2-saturated samples, in agreement with the recorded quantum yields (Table 3). Furthermore, in solution the carbazole series does not exhibit phosphorescence however display a blue shift in the emission (385 to 356) respect to the free ligand.

All compounds (including precursors **P1–P3**) display almost only phosphorescence emission (fluorescence being suppressed) at low temperatures (see Fig. S60†). Under these conditions each series shows a considerable increase in the phosphorescent quantum yield at 77 K, where non-radiative mechanisms are less efficient. In particular, for series 1, the complex **1c** shows the highest quantum yield. In series 2 and 3 the

Open Access Article. Published on 22 January 2025. Downloaded on 1/19/2026 5:16:09 PM.
This article is licensed under a Creative Commons Attribution-NonCommercial 3.0 Unported Licence.

Table 3 Luminescence quantum yields recorded for all the compounds in dichloromethane

Compound	Air-equilibrated samples		N_2-saturated samples		77K[a]
	Φ_{Fl}	Φ_{Ph}	Φ_{Fl}	Φ_{Ph}	Φ_{Ph}
P1	0.04	—	0.04	—	0.01
AuCl(**P1**)	0.01	—	0.01	0.02	0.13
1a	0.01	—	0.01	0.08	0.12
1b	0.01	—	0.01	0.02	0.20
1c	0.01	—	0.01	0.03	0.24
P2	0.01	—	0.08	—	0.03
AuCl(**P2**)	0.01	—	0.01	0.05	0.16
2a	0.01	—	0.01	0.09	0.12
2b	0.01	—	0.01	0.03	0.30
2c	0.01	—	0.01	0.07	0.46
P3	0.03	—	0.03	—	0.29
AuCl(**P3**)	0.01	—	0.02	—	0.11
3a	0.14	—	0.19	—	0.14
3b	0.03	—	0.11	—	0.29
3c	0.09	—	0.13	—	0.41

[a] Φ_{Ph} calculated considering the Ph/Fl ratio and assuming that Φ_{Fl} (RT) ~ Φ_{Fl} (77 K).

highest yields are for complexes **2a** and **3a** in good agreement with the theoretical calculations, where type **a** and **b** complexes present a smaller energy gap (Table 3). These results provide a key insight: the presence of emissive chromophores on both parts of the gold(I) complex does not enhance the sample's emissive properties. Furthermore, a smaller energy gap is observed for type **a** complexes, making emission more favorable when the chromophore is directly coordinated to the metal center.

A new emission band at longer wavelengths appears in all gold(I) complexes from series 1 and 2 when the oxygen is removed from the solution generating a dual emission (Fig. 6). The large Stokes' shift and the vibronically structured shape provide sufficient corroboration to assign this second band to the phosphorescence metal perturbed ^{3}IL transitions. This band is not present for **P1** and **P2** due to the absence of the heavy metal center, responsible for the ISC and T_1 population.[33,42,43]

The phosphorescence emission is more pronounced for the **a** and **c** derivatives (as indicated by the I_P/I_F ratio), due to the direct bonding of the heavy metal to the polyaromatic chromophore, which enhances intersystem crossing (ISC) and facilitates T_1 state population. That is, phosphorescence emission

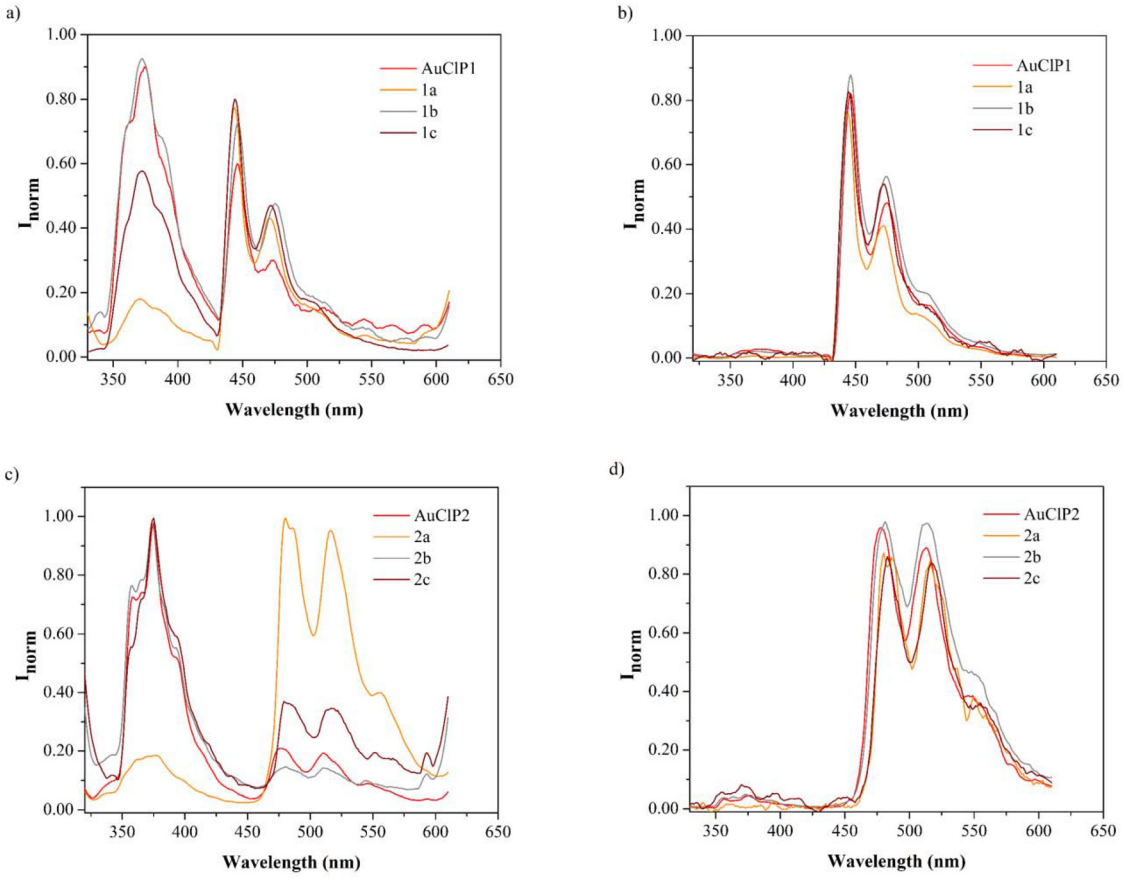

Fig. 6 Emission spectra of (a) series 1 air-equilibrated conditions (b) series 1 N_2-saturated conditions (c) series 2 air-equilibrated conditions (d) series 2 N_2-saturated conditions of PS matrix. Air-equilibrate samples were normalized at the fluorescence maxima.

Open Access Article. Published on 22 January 2025. Downloaded on 1/19/2026 5:16:09 PM.
This article is licensed under a Creative Commons Attribution-NonCommercial 3.0 Unported Licence.

Table 4 Photophysical parameters of PS matrix samples

Quantum yields					Luminescence lifetimes			
	Air-equilibrated samples		N_2-saturated samples		Air-equilibrated samples		N_2-saturated samples	
Compound	Φ_{Fl}	Φ_{Ph}	Φ_{Fl}	Φ_{Ph}	τ_{Fl} (ns)	τ_{Ph} (μs)	τ_{Fl} (ns)	τ_{Ph} (μs)
AuClP1	0.01	<1%	0.01	0.14	14.2	361	—	[a]
1a	<1%	0.01	<1%	0.13	21.1	64	—	526
1b	0.01	0.01	0.01	0.15	12.9	280	—	1239
1c	0.01	0.03	0.01	0.41	18.2	147	—	905
AuClP2	0.01	0.01	0.01	0.09	26.0	263	—	[a]
2a	<1%	0.03	0.02	0.05	43.9	77	—	588
2b	0.01	0.01	0.01	0.30	26.5	187	—	1802
2c	0.02	0.02	0.02	0.24	38.3	62	—	819
AuClP3	0.03	—	0.01	0.01	17.9	—	—	[a]
3a	0.03	—	0.03	0.02	10.1	—	—	324
3b	0.02	—	0.01	0.01	27.7	—	—	[a]
3c	0.03	—	0.01	<1%	10.4	—	—	[a]

[a] Not possible to measure

can be enhanced by the direct coordination of an emissive chromophore to the metal center.

Lifetimes are in the order of a few ns for the fluorescence and hundreds of μs for the corresponding phosphorescence (Table S6†).

In depth investigations on the photophysical properties of the compounds can be done trying to reduce non-radiative processes at room temperature, upon immobilization of the samples in a polymer matrix, such as PS. Interestingly, dual emission is already observed in air-equilibrated samples of Series 1 and 2, unlike in solution (with **1a** and **2a** being the compounds with higher emission phosphorescence intensity), and the emission becomes completely shifted to pure phosphorescence at room temperature when the oxygen is removed from the environment (Fig. 6).

In the case of carbazole derivatives, the gold complexes **3a** and **3b** display phosphorescence at room temperature (under N_2-saturated conditions, Table S7†) which is more favored for **3a**. That means that the competition of internal conversion to ground overrules the radiative pathway for triplet decay, in solution, leading to the absence of phosphorescence. In the polymeric matrix the vibrations are decreased and the radiative pathway for triplet emission becomes competitive restoring phosphorescence.

The quantum yields of all compounds display higher efficiency in the PS films compared to the solutions, confirming that the decrease in internal conversion deactivation pathways for both singlets and triplets due to the decrease in vibrational motions (Table 4). An increase of up to two orders of magnitude in the phosphorescent emission in N_2-saturated conditions is observed, in accordance with much longer lifetimes values recorded.

Conclusions

This study presents a comprehensive investigation into the synthesis, structure, and photophysical properties of gold(I) complexes featuring chromophore-functionalized phosphine ligands. Single-crystal X-ray diffraction confirmed their linear coordination geometries and diverse intermolecular interactions.

A correlation is observed between the crystal structures and the interactions predicted by theoretical calculations. This suggests that when the emissive chromophore is located within the phosphine moiety, centrosymmetric dimers featuring π–π interactions are formed. In contrast, in other configurations, the resulting dimers are less ordered. Therefore, for aggregation studies, it is essential that the structures incorporate chromophores within the phosphine moiety to facilitate these interactions.

Photophysical characterization revealed that luminescence behaviors are heavily influenced by the chromophore type and its coordination environment, with phenanthrene derivatives exhibiting the strongest heavy atom effects, as evidenced by reduced fluorescence intensities and enhanced triplet-state populations. DFT studies corroborated the experimental findings, demonstrating that electronic transitions, S_1–T_1 gaps, and aggregation phenomena significantly impact the observed emission properties. The combination of experimental and computational approaches provides a robust framework for understanding the role of gold(I) in tuning photophysical properties. Future work may explore the potential of these compounds in optoelectronic devices and as models for studying metal-induced photophysical processes.

Experimental section

General procedures

All manipulations have been performed under prepurified N_2 using standard Schlenk techniques. Solvents have been distilled from appropriate drying agents. Commercial reagents 2-bromotriphenylene, 9-phenanthreneboronic acid, carbazole

Open Access Article. Published on 22 January 2025. Downloaded on 1/19/2026 5:16:09 PM.
This article is licensed under a Creative Commons Attribution-NonCommercial 3.0 Unported Licence.

and phenylboronic acid were purchased from Aldrich and used as received.

Physical measurements

Infrared spectra were recorded using a FT-IR 520 Nicolet Spectrophotometer. ^{1}H NMR (δ (TMS) = 0.0 ppm) and ^{31}P{^{1}H} NMR (δ (85% H_3PO_4) = 0.0 ppm) spectra were recorded at 400 or 500 MHz using Varian and Bruker spectrometers at 25 °C (Centres Científics i Tecnològics, Universitat de Barcelona). In the assignation of NMRs spectra, signals denoted with * correspond to the chromophore unit directly linked to the gold (I) metal centre. ES(+) mass spectra were recorded on a Fisons VG Quatro spectrometer (Centres Científics i Tecnològics, Universitat de Barcelona). Absorption spectra were obtained in a 10 mm quartz cuvette in dichloromethane on a Varian Cary 100 Bio UV Spectrophotometer. The emission spectra of the compounds in solution were obtained in a fluorescence quartz cuvette of 10 mm path length, using a Horiba-JobinYbon SPEX Nanolog Spectrofluorimeter (Universitat de Barcelona). Quantum yields have been recorded on Absolute PL quantum yield spectrometer from Hamamatsu Photonics upon excitation the samples at 300–310 nm. Luminescence lifetimes were measured on a JYF-DELTAPRO-NL equipment upon excitation of the samples with a 284 nm NanoLED and collecting the decays through a bandpass filter of 400, 500, or 550 nm, depending on the emission maximum. The best fittings correspond to biexponential decays, and the indicated values correspond to the average considering the respective amplitudes.

The single crystal X-ray data for all crystals were collected at 120 K using an Agilent SuperNova diffractometer with a HyPix-Arc 100 detector using mirror-monochromated Cu-Kα (λ = 1.54184 Å) radiation. The structures were solved by intrinsic phasing (SHELXT)[44] and refined by full-matrix least squares on F^2 using Olex2,[45] utilizing the SHELXL module.[46] Anisotropic displacement parameters were assigned to non-H atoms and isotropic displacement parameters for all H atoms were constrained to multiples of the equivalent displacement parameters of their parent atoms with U_{iso}(H) = 1.2 U_{eq}(C) of their respective parent atoms. The crystal data and experimental details for the data collections of **1a**, **1b**, **3a**, and **3b** are given in Tables S1–S4,† respectively. Deposition numbers 2409503 (**1a**), 2409504 (**1b**), 2409505 (**3a**), and 2409506 (**3b**)† contain the supplementary crystallographic data for this paper. These data are provided free of charge by the joint Cambridge Crystallographic Data Centre and Fachinformationszentrum Karlsruhe Access Structures service.

Theoretical methods

The geometries of all compounds in this study were fully optimized at the RI-BP86-D4/def2-TZVP level of theory[47] (a–d) using the Turbomole 7.7 program.[48] Frequency calculations were conducted for both monomers and dimers to confirm their true minimum nature and to estimate entropic contributions. Gibbs free energies were calculated at room temperature. Solvent effects (dichloromethane, DCM) were accounted for using the COSMO model,[49] a variant of dielectric continuum solvation models. Time-dependent DFT (TD-DFT) calculations were performed to compute 100 excited states using the CAM-B3LYP functional[50] using the ORCA 5.0 program,[51] with solvent effects incorporated *via* the CPCM solvation model.[52] The gold's basis set used effective core potential with scalar relativistic effects (RECP).[53]

Synthesis and characterization

Synthesis of phosphine ligands

*Diphenyl(triphenylen-2-yl)phosphane (**P1**).* The synthesis of **P1** refers to literature reports.[1] A solution of 2-bromotriphenylene (0.359 g, 1.17 mmol) in 10 mL of THF was cooled to −78 °C and *n*-butyllithium (0.80 mL, 1.25 mmol) was added and stirred for 1 h. Next, $P(Ph)_2Cl$ (0.20 mL, 1.28 mmol) was added dropwise. After stirring 1 h at −78 °C the refrigeration was stopped, and the reaction mixture was stirred overnight. Subsequently deionized water (20 mL) was added and THF was removed by reduced pressure evaporation. The resulting aqueous phase was extracted with dichloromethane (3 × 20 mL). Then the combined organic phase was dried over anhydrous sodium sulfate. The solvent was evaporated, and the crude oil obtained was purified by silica gel column chromatography and DCM/Hex (2 : 3). Yield 31%. ^{1}H NMR (400 MHz, $CDCl_3$, ppm): δ 8.68–8.58 (m, 5H), 8.40 (ddd, J = 8.0, 1.5, 0.8 Hz, 1H), 7.70–7.51 (m, 6H), 7.45–7.35 (m, 9H). ^{31}P{^{1}H} NMR (162 MHz, $CDCl_3$, ppm): δ −4.92. MALDI-TOF(+) *m*/*z*: 413.142 ([M + H]$^+$, calcd 413.1454). IR ($\bar{\nu}$, cm^{-1}): ν(=C–H) 3059, ν(C=C) 1436, δ(C–H Ph) 727–680 cm^{-1}.

*Phenanthren-9-yldiphenylphosphane (**P2**).* The synthesis of **P2** was performed by following the same procedure as **P1** but using 9-bromophenanthrene (0.300 g, 1.17 mmol) and for chromatographic purification DCM/Hex (1 : 4) was used. Yield 37%. ^{1}H NMR (400 MHz, $CDCl_3$, ppm): δ 8.73 (d, J = 7.5 Hz, 1H), 8.68 (d, J = 7.8 Hz, 1H), 8.47–8.43 (m, 1H), 7.68–7.60 (m, 3H), 7.56–7.49 (m, 2H), 7.41–7.32 (m, 10H), 7.24 (d, J = 5.2 Hz, 1H). ^{31}P{^{1}H} NMR (162 MHz, $CDCl_3$, ppm): δ −12.94. MALDI-TOF(+) *m*/*z*: 363.101 ([M + H]$^+$, calcd 363.1297). IR ($\bar{\nu}$, cm^{-1}): ν(=C–H) 3060, ν(C=C) 1435, δ(C–H Ph) 740–687 cm^{-1}.

*9,9′-(Phenylphosphanediyl) bis (9H-carbazole) (**P3**).* The synthesis of **P3** refers to literature reports.[2] A solution of carbazole (0.520 g, 3.11 mmol) in 10 mL of THF/Hex (1 : 1) was cooled to −78 °C and *n*-butyllithium (2.0 mL, 3.20 mmol) was added and stirred for 1 h. Next, the temperature was allowed to warm up to −20 °C and $PPhCl_2$ (0.21 mL, 1.55 mmol) was added dropwise. After stirred for 1 h the refrigeration was stopped, and the reaction mixture was stirred overnight. The solvent was removed under vacuum and the white solid obtained was purified by silica gel column chromatography (30% DCM–70% Hex). Yield 52%. ^{1}H NMR (500 MHz, $CDCl_3$, ppm): δ 8.05–8.00 (m, 4H), 7.60–7.55 (m, 4H), 7.54–7.48 (m, 3H), 7.46–7.41 (m, 2H), 7.30–7.23 (m, 8H). ^{31}P{^{1}H} NMR (162 MHz, $CDCl_3$, ppm): δ 51.80. MALDI-TOF(+) *m*/*z*: 441.1203 ([M + H]$^+$, calcd 441.1515). IR ($\bar{\nu}$, cm^{-1}): ν(=C–H) 3064, ν(C=C) 1428, ν(C–N) 1334, δ(C–H Ph) 747 cm^{-1}.

Synthesis of the phosphine gold chlorido precursors

*Gold chloride triphenylene phosphane ([AuCl(**P1**)]).* [AuCl(tht)] (0.078 g, 0.24 mmol) was added to a previously prepared solu-

Open Access Article. Published on 22 January 2025. Downloaded on 1/19/2026 5:16:09 PM.
This article is licensed under a Creative Commons Attribution-NonCommercial 3.0 Unported Licence.

tion of **P1** (0.100 g, 0.24 mmol) in dichloromethane (5 mL). The mixture was stirred for 1 h. The product was precipitated by the addition of hexane (10 mL). The obtained white solid was filtered and dried *in vacuo*. Yield 91%. ^{1}HNMR (400 MHz, $CDCl_3$, ppm): δ 8.86 (dd, J = 15.3, 1.7 Hz, 1H, H_1), 8.73 (dd, J = 8.5, 2.5 Hz, 1H), 8.70–8.63 (m, 3H), 8.40–8.37 (m, 1H), 7.77–7.49 (m, 15H). ^{31}P{^{1}H} NMR (162 MHz, $CDCl_3$, ppm): δ 33.54. IR ($\bar{\nu}$, cm^{-1}): ν(=C–H) 3052, ν(C=C) 1475–1448, δ(C–H Ph) 760–693 cm^{-1}.

*Gold chloride phenanthrene phosphane ([AuCl(**P2**)]).* The synthesis of [AuCl(**P2**)] was performed by following the same procedure as [AuCl(**P1**)] by substitution of **P1** for **P2** (0.100 g, 0.28 mmol). Yield 82%. ^{1}H-NMR (400 MHz, $CDCl_3$, ppm): δ 8.78–8.75 (m, 1H, H_6), 8.71 (d, J = 8.6 Hz, 1H, H_5), 8.47 (m, 1H, H_9), 7.79–7.72 (m, 1H), 7.71–7.62 (m, 6H), 7.61–7.56 (m, 3H), 7.55–7.47 (m, 5H), 7.30 (d, J = 15.6 Hz, 1H, H_1). ^{31}P{^{1}H} NMR (162 MHz, $CDCl_3$, ppm): δ 27.22. IR ($\bar{\nu}$, cm^{-1}): ν(=C–H) 3052, ν(C=C) 1435, δ(C–H Ph) 740 cm^{-1}.

*Gold chloride carbazole phosphane ([AuCl(**P3**)]).* The synthesis of [AuCl(**P3**)] was performed by following the same procedure as [AuCl(**P1**)] by substitution of **P1** for **P3** (0.100 g, 0.23 mmol). Yield 96%. ^{1}H-NMR (400 MHz, $CDCl_3$, ppm): δ 8.08–8.04 (m, 4H, H_4), 8.00–7.93 (m, 2H, *o*-Ph), 7.83–7.77 (m, 1H, *p*-Ph), 7.66–7.60 (m, 2H, *m*-Ph), 7.33 (ddd, J = 7.9, 7.2, 1.0 Hz, 4H, H_3), 7.26 (d, J = 8.4 Hz, 4H, H_1), 7.18 (ddd, J = 8.4, 7.2, 1.3 Hz, 4H, H_2). ^{31}P{^{1}H} NMR (162 MHz, $CDCl_3$, ppm): δ 72.5. ^{13}C{^{1}H} NMR (100 MHz, $CDCl_3$, ppm): δ 141.2 (d, J = 4 Hz, C_6), 135.0 (d, J = 3 Hz, *p*-Ph), 133.8 (d, J = 19 Hz, *o*-Ph), 130.3 (d, J = 14 Hz, *m*-Ph), 128.9 (d, J = 76 Hz, *ipso*-Ph), 127.2 (s, C_2), 127.1 (C_5), 123.4 (C_3), 120.6 (C_4), 113.8 (d, J = 6.5 Hz, C_1). IR ($\bar{\nu}$, cm^{-1}): ν(=C–H) 3052, ν(C=C) 1428, ν(C–N) 1334, δ(C–H Ph) 740 cm^{-1}.

Synthesis of the complexes

(1a). Compound **1a** was synthesized according to the literature method.[3] *Part A*. Synthesis of 4,4,5,5-Tetramethyl-2-(triphenylen-2-yl)-1,3,2-dioxaborolane (TPBpin). The synthesis of TPBpin was carried out according to the literature.[18] 2-bromotriphenylene (0.300 g, 0.98 mmol), bis(pinacolato) diborate (0.372 g, 1.46 mmol), [1,10 bis(diphenylphosphino)ferrocene] dichloropalladium(II) (0.0294 g, 0.04 mmol), and potassium acetate (0.243 g, 2.96 mmol) were dissolved in anhydrous 1,4-dioxane (20 ml) and refluxed under nitrogen for 24 h. The reaction mixture was diluted with ethyl acetate and washed with brine and water (2 × 10 mL). Then, the organic layer was extracted and dried over anhydrous $MgSO_4$. After evaporation of the solvent, the crude product was purified by column chromatography on silica gel using a dichloromethane/hexane (1 : 1) mixed eluent. A pale-yellow powder product was obtained after purification Yield 13%. ^{1}H NMR (500 MHz, $CDCl_3$, ppm): δ 9.14 (s, 1H), 8.82 (m, 1H), 8.67 (m, 4H), 8.06 (dd, J = 8.2, 1.2 Hz, 1H), 7.67 (m, 4H), 1.43 (s, 12H). IR ($\bar{\nu}$, cm^{-1}): ν(C–H) 2974, δ(C–H) 1804, ν(B–O) 1362, δ(C–H Ph) 751–682 cm^{-1}. *Part B*. Cs_2CO_3 (0.032 g, 0.10 mmol) and TPBpin (0.029 g, 0.08 mmol) were suspended in isopropyl alcohol (10 mL) and [AuCl(PPh_3)] (0.032, 0.06 mmol) was added to the suspension. After 5 days stirring at RT in the dark, the solvent was evaporated *in vacuo* and the residue was extracted with dichloromethane (2 × 10 mL). The obtained solution was filtered through Celite then the solvent was removed, and a white solid powder was obtained. Yield 88%. ^{1}H NMR (500 MHz, $CDCl_3$, ppm): δ 8.94 (d, J = 6.0 Hz, 1H, H_1*), 8.82–8.78 (m, 1H), 8.69–8.61 (m, 3H), 8.56 (dd, J = 8.2, 1.6 Hz, 1H, H_3*), 7.92 (ddd, J = 8.0, 4.9, 0.9 Hz, 1H, H_2*), 7.70–7.64 (m, 6H), 7.64–7.57 (m, 4H), 7.56–7.48 (m, 9H). ^{31}P{^{1}H} NMR (162 MHz, $CDCl_3$, ppm): δ 43.25. ES-MS (+) m/z: 709.1292 ([M + Na]$^+$, calcd 709.1335), 1145.2009 ([2 M − L]$^+$, calcd 1145.2015). IR ($\bar{\nu}$, cm^{-1}): ν(=C–H) 3044, ν(C=C) 1435, δ(C–H Ph) 750–693 cm^{-1}.

(2a). The synthesis of **2a** was performed by following the same procedure as **1a**: Cs_2CO_3 (0.176 g, 0.54 mmol), 9-phenanthracenylboronic acid (0.100 g, 0.45 mmol) and [AuCl(PPh_3)] (0.178, 0.36 mmol). Yield 74%. ^{1}H NMR (500 MHz, $CDCl_3$, ppm): δ 8.74–8.71 (m, 1H, H_6*), 8.70–8.67 (m, 1H, H_9*), 8.66–8.63 (m, 1H, H_5*), 8.00 (d, J = 6.5 Hz, 1H, H_1*), 7.85–7.79 (m, 1H, H_2*), 7.73–7.65 (m, 6H, Ph), 7.59–7.48 (m, 13H). ^{31}P{^{1}H} NMR (162 MHz, $CDCl_3$, ppm): δ 44.26. ES-MS (+) m/z: 637.1360 ([M + H]$^+$, calcd 637.1359), 659.1177 ([M + Na]$^+$, calcd 659.1179). IR ($\bar{\nu}$, cm^{-1}): ν(=C–H) 3044, ν(C=C) 1435, δ(C–H Ph) 740–687 cm^{-1}.

(3a). A solution of carbazole (0.027 g, 0.16 mmol) in dichloromethane (5 mL) was added to a solution of KOH (0.027 g, 0.48 mmol) in methanol (2 mL). The reaction mixture was stirred for 30 min at RT. Then a solution of [AuCl(PPh_3)] (0.079 g, 0.16 mmol) in dichloromethane was added. After 1 h stirring the solvent was evaporated *in vacuo* and the remaining solid was dissolved in dichloromethane (5 mL) and filtered through Celite. The solvent was removed, and the white solid was recrystallized with dichloromethane/hexane to obtain the pure product. Yield 89%. ^{1}H NMR (500 MHz, $CDCl_3$, ppm): δ 8.14 (m, 2H, H_4*), 7.77 (dd, J = 8.0, 0.8 Hz, 2H, H_1*), 7.70–7.63 (m, 6H Ph), 7.59–7.51 (m, 9H, Ph), 7.34 (ddd, J = 8.2, 7.0, 1.3 Hz, 2H, H_2*), 7.09 (ddd, J = 7.9, 7.0, 1.0 Hz, 2H, H_3*). ^{31}P{^{1}H} NMR (162 MHz, $CDCl_3$, ppm): δ 33.71. ^{13}C{^{1}H} NMR (100 MHz, $CDCl_3$, ppm): δ 149.3 (s, C_6*), 134.4 (d, J = 13.6 Hz, *o*-Ph), 132.1 (d, J = 2.6 Hz, *p*-Ph), 129.5 (d, J = 11.6 Hz, *m*-Ph), 129.3 (d, J = 60 Hz, *ipso*-Ph), 124.2 (d, J = 2.5 Hz, C_5*), 124.1 (C_2*), 120.0 (C_4*), 116.8 (C_3*), 113.5 (C_1*). MALDI-TOF(+) m/z: 625.1 ([M]$^+$, calcd 625.1234). IR ($\bar{\nu}$, cm^{-1}): ν(=C–H) 3064, ν(C=C) 1441, ν(C–N) 1235, δ(C–H Ph) 747–687 cm^{-1}.

(1b). Cs_2CO_3 (0.114 g, 0.35 mmol) and phenylboronic acid (0.036 g, 0.29 mmol) were suspended in isopropyl alcohol (10 mL) and a solution of [AuCl(**P1**)] (0.050 g, 0.08 mmol) in dichloromethane (5 mL) was added to the suspension. After 2 days stirring at 40 °C the precipitated product was filtered and dried *in vacuo*. Next, the solid was dissolved in dichloromethane (5 mL) and filtered through Celite. The solvent was removed, and a white solid powder was obtained. Yield 18%. ^{1}H NMR (400 MHz, $CDCl_3$, ppm): δ 8.98 (dd, J = 13.7, 1.7 Hz, 1H, H_1), 8.75–8.70 (dd, J = 8.5, 2.2 Hz, 1H, H_3), 8.69–8.63 (m, 3H), 8.45–8.40 (m, 1H), 7.81–7.75 (m, 1H, H_2), 7.73–7.60 (m, 10H), 7.57–7.47 (m, 6H), 7.35–7.30 (m, 2H, Ph–Au H_{15} or H_{16}), 7.15–7.09 (m, 1H, Ph–Au H_{17}). ^{31}P{^{1}H} NMR (162 MHz, $CDCl_3$,

Open Access Article. Published on 22 January 2025. Downloaded on 1/19/2026 5:16:09 PM. This article is licensed under a Creative Commons Attribution-NonCommercial 3.0 Unported Licence.

ppm): δ 43.98. ES-MS (+) *m/z*: 1395.2715 ([2 M + Na]$^+$, calcd 1395.2773), 1295.2443 ([2 M − Ph]$^+$, calcd 1295.2484). IR ($\bar{\nu}$, cm^{-1}): ν(=C–H) 3058, ν(C=C) 1635–1435, δ(C–H Ph) 820–687 cm^{-1}.

(2b). The synthesis of **2b** was performed by following a similar procedure as **1b**: Cs_2CO_3 (0.020 g, 0.06 mmol), phenylboronic acid (0.01 g, 0.05 mmol) and [AuCl(**P2**)] (0.02 g, 0.04 mmol). In this synthesis the reaction mixture was stirred for 5 days at RT. Yield 63%. ^{1}H NMR (500 MHz, $CDCl_3$, ppm): δ 8.79–8.68 (m, 3H, H_5, H_6, H_9), 7.78–7.66 (m, 6H), 7.63 (dd, J = 7.9, 1.5 Hz, 1H), 7.60–7.45 (m, 10H), 7.30 (d, J = 13.3 Hz, 1H, H_1), 7.26–7.23 (m, 2H), 7.11–7.04 (m, 1H, *p*-PhAu). ^{31}P{^{1}H} NMR (162 MHz, $CDCl_3$, ppm): δ 39.53. ES-MS (+) *m/z*: 659.1161 ([M + Na]$^+$, calcd 659.1179), 1195.2159 ([2 M − Ph]$^+$, calcd 1195.2171). IR ($\bar{\nu}$, cm^{-1}): ν(=C–H) 3052, ν(C=C) 1435, δ(C–H Ph) 753–687 cm^{-1}.

(3b). The synthesis of **3b** was performed by following the same procedure as **2b**: Cs_2CO_3 (0.014 g, 0.04 mmol), phenylboronic acid (0.004 g, 0.04 mmol) and [AuCl(**P3**)] (0.020 g, 0.03 mmol). Yield 38%. ^{1}H NMR (500 MHz, $CDCl_3$, ppm): δ 8.05 (d, J = 6.7 Hz, 4H, H_4), 8.01 (m, 2H, *o*-Ph), 7.73 (m, 1H, *p*-Ph), 7.62–7.56 (m, 2H, *m*-Ph), 7.53 (d, J = 8.5 Hz, 4H, H_1), 7.43–7.39 (m, 2H, *o*-PhAu), 7.33–7.28 (m, 4H, H_3), 7.24–7.16 (m, 6H, H_2, *m*-PhAu), 7.09–7.04 (m, 1H, *p*-PhAu). ^{31}P{^{1}H} NMR (162 MHz, $CDCl_3$, ppm): δ 100.79. ES-MS (+) *m/z*: 737.1381 ([M + Na]$^+$, calcd 737.1397), 1351.2601 ([2 M − Ph]$^+$, calcd 1351.2607). IR ($\bar{\nu}$, cm^{-1}): ν(=C–H) 3058, ν(C=C) 1435, ν(C–N) 1201, δ(C–H Ph) 740 cm^{-1}.

(1c). Cs_2CO_3 (0.040 g, 0.12 mmol) and **P1** (0.035 g, 0.10 mmol) were suspended in isopropyl alcohol (10 mL) and a solution of [AuCl(**P1**)] (0.026 g, 0.04 mmol) in dichloromethane (5 mL) was added to the suspension. After 5 days stirring at RT the precipitated product was filtered and dried *in vacuo*. Next, the solid was dissolved in dichloromethane (5 mL) and filtered through Celite. The solvent was evaporated *in vacuo* and the residue was washed with methanol (2 × 5 mL). The solvent was removed, and an orange solid powder was obtained. Yield 16%. ^{1}H NMR (400 MHz, $CDCl_3$, ppm): δ 9.07 (dd, J = 13.9, 1.7 Hz, 1H, H_1), 9.01 (d, J = 6.0 Hz, 1H, H_1*), 8.86–8.81 (m, 1H), 8.77 (dd, J = 8.6, 2.2 Hz, 1H, H_3), 8.71–8.62 (m, 6H), 8.60 (dd, J = 8.2, 1.6 Hz, 1H, H_3*), 8.51–8.47 (m, 1H), 7.98 (ddd, J = 8.0, 4.9, 0.8 Hz, 1H, H_2*), 7.84 (ddd, J = 10.2, 8.5, 1.6 Hz, 1H, H_2), 7.81–7.50 (m, 18H). ^{31}P{^{1}H} NMR (162 MHz, $CDCl_3$, ppm): δ 44.00. MALDI-TOF(+) *m/z*: 859.1785 ([M + Na]$^+$, calcd 859.1805), 413.1457 ([M − Au − L]$^+$, calcd 412.1381). IR ($\bar{\nu}$, cm^{-1}): ν(=C–H) 2962, ν(C=C) 1433, δ(C–H Ph) 792–690 cm^{-1}.

(2c). The synthesis of **2c** was performed by following a similar procedure as **1c**: Cs_2CO_3 (0.062 g, 0.19 mmol), 9-Phenanthracenylboronic acid (0.034 g, 0.16 mmol) and [AuCl(**P2**)] (0.050, 0.08 mmol). Yield 12%. ^{1}H NMR (500 MHz, $CDCl_3$, ppm): δ 8.90 (d, J = 8.2 Hz, 1H), 8.80 (d, J = 8.5 Hz, 1H), 8.74 (d, J = 8.4 Hz, 1H), 8.69 (d, J = 7.9 Hz, 1H), 8.64–8.57 (m, 2H), 7.95 (d, J = 6.4 Hz, 1H, H_1*), 7.85–7.71 (m, 7H), 7.67–7.44 (m, 13H), 7.36 (d, J = 13.6 Hz, 1H, H_1). ^{31}P{^{1}H} NMR (162 MHz, $CDCl_3$, ppm): δ 40.67. MALDI-TOF(+) *m/z*: 737.1662 ([M + H]$^+$, calcd 737.1672), 759.1483 ([M + Na]$^+$, calcd 759.1492). IR ($\bar{\nu}$, cm^{-1}): ν(=C–H) 3053, ν(C=C) 1434, δ(C–H Ph) 741–691 cm^{-1}.

(3c). Carbazole (0.013 g, 0.08 mmol) and [AuCl(**P3**)] (0.050 g, 0.07 mmol) were added to a solution of K_2CO_3 (0.031 g, 0.22 mmol) in acetone (0.5 mL). The reaction mixture was stirred for 24 h at RT. Then the solvent was evaporated *in vacuo* and the remaining solid was recrystallized with dichloromethane/hexane to obtain the yellow pure product. Yield 33%. ^{1}H NMR (500 MHz, $CDCl_3$, ppm): δ 8.13–8.02 (m, 8H, H_4, H_4*, *o*-Ph), 7.87–7.81 (m, 1H, *p*-Ph), 7.72–7.66 (m, 2H, *m*-Ph), 7.48 (d, J = 8.4 Hz, 4H, H_1), 7.46–7.41 (m, 2H, H_1*), 7.37 (*p*t, J = 7.5 Hz, 3H, H_3), 7.26–7.21 (m, 6H, H_2, H_2*), 7.06 (*p*t, 7.4 Hz, 2H, H_3*). ^{31}P{^{1}H} NMR (202 MHz, $CDCl_3$, ppm): δ 79.16. ^{13}C{^{1}H} NMR (125 MHz, $CDCl_3$, ppm): δ 149.0 (s, C_6*), 141.5 (d, J = 4.5 Hz, C_6), 134.9 (*p*-Ph), 133.8 (d, J = 19 Hz, *o*-Ph), 130.5 (d, J = 13.5 Hz, *m*-Ph), 129.2 (d, J = 73 Hz, *ipso*-Ph), 127.3 (C_5), 127.2 (C_2), 124.2 (C_2*), 123.5 (C_3), 120.7 (C_4), 119.9 (C_4*), 117.0 (C_3*), 113.9 (d, J = 6.2 Hz, C_1), 113.3 (C_1*). MALDI-TOF(+) *m/z*: 804.1511 ([M + H]$^+$, calcd 804.1837), 1077.1874 ([Au(P3)$_2$]$^+$, calcd 1078.2622). IR ($\bar{\nu}$, cm^{-1}): ν(=C–H) 2961, ν(C=C) 1450, ν(C–N) 1195, δ(C–H Ph) 743–694 cm^{-1}.

Data availability

The datasets supporting this article, including experimental data, computational files, and characterization data, are available in the ESI.† Additional data are available from the corresponding author upon reasonable request.

Conflicts of interest

There are no conflicts to declare.

Acknowledgements

The authors are grateful to Projects PID2020-115637GB-I00, PID2022-139296NB-I00 and PID2023-148453NB-I00 funded by the Ministerio de Ciencia, Innovación y Universidades of Spain MCIU/AEI/10.13039/501100011033 and FEDER, UE. This article is based upon work from COST Action CA22131, LUCES Supramolecular LUminescent Chemosensors for Environmental Security, supported by COST (European Cooperation in Science and Technology). Also acknowledges IFARHU-SENACYT program in Panamá for the grant no. 270-2022-112 as Ph.D. Scholarship.

References

1 V. R. Naina, S. Gillhuber, C. Ritschel, D. Jin, Shubham, S. Lebedkin, C. Feldmann, F. Weigend, M. M. Kappes and P. W. Roesky, Dye Induced Luminescence Properties of Gold(I) Complexes with near Unity Quantum Efficiency, *Angew. Chem., Int. Ed.*, 2024, e202414517.

Open Access Article. Published on 22 January 2025. Downloaded on 1/19/2026 5:16:09 PM.
This article is licensed under a Creative Commons Attribution-NonCommercial 3.0 Unported Licence.

2 E. E. Langdon-Jones and S. J. A. Pope, Recent developments in gold(I) coordination chemistry: luminescence properties and bioimaging opportunities, *Chem. Commun.*, 2014, **50**, 10343–10354.
3 Y. Lu, X. Ma, X. Chang, Z. Liang, L. Lv, M. Shan, Q. Lu, Z. Wen, R. Gust and W. Liu, Recent development of gold(I) and gold(III) complexes as therapeutic agents for cancer diseases, *Chem. Soc. Rev.*, 2022, **51**, 5518–5556.
4 A. Casini and S. R. Thomas, The Beauty of Gold: Knowledge of Mechanisms Leads to Different Applications of Organogold Compounds in Medicine and Catalysis, *Chem. Lett.*, 2021, **50**, 1516–1522.
5 R. P. Herrera and M. C. Gimeno, Main Avenues in Gold Coordination Chemistry, *Chem. Rev.*, 2021, **121**, 8311–8363.
6 S. Avula, B. H. Jhun, U. Jo, S. Heo, J. Y. Lee and Y. You, Achieving Long-Wavelength Electroluminescence Using Two-Coordinate Gold(I) Complexes: Overcoming the Energy Gap Law, *Adv. Sci.*, 2023, 2305745.
7 N. M. W. Wu, M. Ng and V. W. W. Yam, Photocontrolled Multiple-State Photochromic Benzo[b]phosphole Thieno [3,2-b]phosphole-Containing Alkynylgold(I) Complex via Selective Light Irradiation, *Nat. Commun.*, 2022, **13**, 33.
8 (*a*) S. Burguera, A. Bauzá and A. Frontera, A novel approach for estimating the strength of argentophilic and aurophilic interactions using QTAIM parameters, *Phys. Chem. Chem. Phys.*, 2024, **26**, 16550–16560; (*b*) A. Frontera and L. Rodríguez, Exploring aurophilic interactions in P,C–Au (I)–Y complexes: Pathways to supramolecular aggregation, *Adv. Inorg. Chem.*, 2024, **84**, 55–104.
9 A. de Aquino, F. J. Caparrós, G. Aullón, K.-N. Truong, K. Rissanen, J. C. Lima and L. Rodríguez, Development of gold(I) phosphorescent tweezers for sensing applications, *Dalton Trans.*, 2022, **51**, 16282–16291.
10 M. Gil-Moles and M. C. Gimeno, The Therapeutic Potential in Cancer of Terpyridine-Based Metal Complexes Featuring Group 11 Elements, *ChemMedChem*, 2024, e202300645.
11 Q. Zheng, S. Borsley, G. S. Nichol, F. Duarte and S. L. Cockroft, The Energetic Significance of Metallophilic Interactions, *Angew. Chem., Int. Ed.*, 2019, **58**, 12617–12623.
12 H. Schmidbaur and H. G. Raubenheimer, Excimer and Exciplex Formation in Gold(I) Complexes Preconditioned by Aurophilic Interactions, *Angew. Chem., Int. Ed.*, 2020, **59**, 14748–14771.
13 A. Pinto and L. Rodríguez, Gold(I) complexes as powerful photosensitizers – a visionary frontier perspective, *Dalton Trans.*, 2024, **53**, 13716–13725.
14 J. C. Lima and L. Rodríguez, Highlights on Gold TADF Complexes, *Inorganics*, 2019, **7**, 124.
15 M. Pujadas and L. Rodríguez, Luminescent phosphine gold (I) alkynyl complexes. Highlights from 2010 to 2018, *Coord. Chem. Rev.*, 2020, **408**, 213179.
16 J. C. Lima and L. Rodríguez, Applications of gold(I) alkynyl systems: a growing field to explore, *Chem. Soc. Rev.*, 2011, **40**, 5442–5456.
17 C. Sobrerroca, I. Angurell, A. de Aquino, G. Romo, C. Jubert and L. Rodríguez, Mono- and Dinuclear Gold(I) Coumarin Complexes: Luminescence Studies and Singlet Oxygen Production, *ChemPlusChem*, 2023, **88**, e202300020.
18 L. Luciani, N. Sargentoni, C. Graiff, M. Monge, M. Rodríguez-Castillo, J. M. López de Luzuriaga and R. Galassi, Mechanochemical preparation of strongly emissive monosubstituted triarylphosphane gold(I) compounds activated by hydrogen bonding driven aggregations, *RSC Adv.*, 2023, **13**, 25425.
19 M. Osawa, M. Hoshino, T. Wada, Y. Araki and O. Ito, Phosphorous atom induced intramolecular charge transfer fluorescence in 9-diphenylphosphinophenanthrene, *Chem. Phys. Lett.*, 2006, **427**, 338–342.
20 Z. Zhao, G. Yu, Q. Chang, X. Liu, Y. Liu, L. Wang, Z. Liu, Z. Bian, W. Liu and C. Huang, Carbazolylphosphines and carbazolylphosphine oxides: facilely synthesized host materials with tunable mobilities and high triplet energy levels for blue phosphorescent OLEDs, *J. Mater. Chem. C*, 2017, **5**, 7344–7351.
21 M. Osawa, M. Hoshino, M. Akita and T. Wada, Synthesis and Characterization of Phenanthrylphosphine Gold Complex: Observation of Au-Induced Blue-Green Phosphorescence at Room Temperature, *Inorg. Chem.*, 2005, **44**, 1157–1159.
22 A. de Aquino, J. S. Ward, K. Rissanen, G. Aullón, J. C. Lima and L. Rodríguez, Intra- vs Intermolecular Aurophilic Contacts in Dinuclear Gold(I) Compounds: Impact on the Population of the Triplet Excited State, *Inorg. Chem.*, 2022, **61**, 20931–20941.
23 M. E. Şahin, F. Biryan, E. Çalışkan and K. Koran, Coumarin–Phosphazenes: Enhanced Photophysical Properties from Hybrid Materials, *Inorg. Chem.*, 2024, **63**, 11006–11020.
24 V. R. Naina, A. K. Singh, P. Rauthe, S. Lebedkin, M. T. Gamer, M. M. Kappes, A.-N. Unterreiner and P. W. Roesky, Phase-Dependent Long Persistent Phosphorescence in Coumarin-Phosphine-Based Coinage Metal Complexes, *Chem. – Eur. J.*, 2023, e202300497.
25 V. R. Naina, A. K. Singh, Shubham, J. Krämer, M. Iqbala and P. W. Roesky, Synthesis of luminescent coumarin-substituted phosphinoamide-bridged polynuclear gold(I) metallacycles and reactivity studies, *Inorg. Chem. Front.*, 2024, **11**, 6079–6088.
26 A. Fukazawa, S. Suda, M. Taki, E. Yamaguchi, M. Grzybowski, Y. Sato, T. Higashiyama and S. Yamaguchi, Phospha-fluorescein: a red-emissive fluorescein analogue with high photobleaching resistance, *Chem. Commun.*, 2016, **52**, 1120–1123.
27 X. Zhou, R. Lai, J. R. Beck, H. Li and C. I. Stains, Nebraska Red: a phosphinate-based near-infrared fluorophore scaffold for chemical biology applications, *Chem. Commun.*, 2016, **52**, 12290–12293.
28 L. H. Davies, B. Stewart, R. W. Harrington, W. Clegg and L. J. Higham, Air-Stable, Highly Fluorescent Primary Phosphanes, *Angew. Chem., Int. Ed.*, 2012, **51**, 4921–4924.
29 X. He, J. Borau-Garcia, A. Y. Y. Woo, S. Trudel and T. Baumgartner, Dithieno[3,2-c:2′,3′-e]-2,7-diketophosphe-

Open Access Article. Published on 22 January 2025. Downloaded on 1/19/2026 5:16:09 PM.
This article is licensed under a Creative Commons Attribution-NonCommercial 3.0 Unported Licence.

pin: A Unique Building Block for Multifunctional π-Conjugated Materials, *J. Am. Chem. Soc.*, 2013, **135**, 1137–1147.

30 T. Agou, J. Kobayashi and T. Kawashima, Dibenzophosphaborin: A Hetero-π-conjugated Molecule with Fluorescent Properties Based on Intramolecular Charge Transfer between Phosphorus and Boron Atoms, *Org. Lett.*, 2005, **7**, 4373–4376.

31 Z. An, C. Zheng, Y. Tao, R. Chen, H. Shi, T. Chen, Z. Wang, H. Li, R. Deng, X. Liu and W. Huang, Stabilizing Triplet Excited States for Ultralong Organic Phosphorescence, *Nat. Mater.*, 2015, **14**, 685–690.

32 F. J. L. Ingner, A. C. Schmitt, A. Orthaber, P. J. Gates and L. T. Pilarski, Mild and Efficient Synthesis of Diverse Organo-AuI-L Complexes in Green Solvents, *ChemSusChem*, 2020, **13**, 2032–2037.

33 A. de Aquino, F. J. Caparrós, G. Aullón, J. S. Ward, K. Rissanen, Y. Jung, H. Choi, J. C. Lima and L. Rodríguez, Effect of Gold(I) on the Room-Temperature Phosphorescence of Ethynylphenanthrene, *Chem. – Eur. J.*, 2021, **27**, 1810–1820.

34 N. V. Tzouras, T. Scattolin, A. Gobbo, S. Bhandary, F. Rizzolio, E. Cavarzerani, V. Canzonieri, K. Van Hecke, G. C. Vougioukalakis and S. P. Nolan, A Green Synthesis of Carbene-Metal-Amides (CMAs) and Carboline-Derived CMAs with Potent in Vitro and Ex Vivo Anticancer Activity, *ChemMedChem*, 2022, **17**, e202200135.

35 (*a*) D. V. Partyka, M. Zeller, A. D. Hunter and T. G. Gray, Relativistic functional groups: aryl carbon-gold bond formation by selective transmetalation of boronic acids, *Angew. Chem., Int. Ed.*, 2006, **45**, 8188–8191; (*b*) L. Gao, M. A. Peay, D. V. Partyka, J. B. Updegraff, T. S. Teets, A. J. Esswein, M. Zeller, A. D. Hunter and T. G. Gray, Mono- and Di-Gold(I) Naphthalenes and Pyrenes: Syntheses, Crystal Structures, and Photophysics, *Organometallics*, 2009, **28**, 5669–5681.

36 (*a*) M. Ferrer, A. Gutiérrez, M. Martínez, C. Da Silva, A. V. G. Netto, L. Rodríguez, G. Romo-Islas, F. Pan and K. Rissanen, Base-Assisted Synthesis of 4-Pyridinate Gold(I) Metallaligands: A Study of Their Use in Self-Assembly Reactions, *Dalton Trans.*, 2021, **50**, 8154–8166; (*b*) A. de Aquino, F. J. Caparrós, K.-N. Truong, K. Rissanen, M. Ferrer, Y. Jung, H. Choi, J. C. Lima and L. Rodríguez, Gold(I)-doped films: new routes for efficient room temperature phosphorescent materials, *Dalton Trans.*, 2021, **50**, 3806–3815.

37 R. Nandy and S. Sankararaman, Donor-Acceptor Substituted Phenylethynyltriphenylenes - Excited State Intramolecular Charge Transfer, Solvatochromic Absorption and Fluorescence Emission, *Beilstein J. Org. Chem.*, 2010, **6**, 992–1001.

38 F. Liu, G. Cao, Z. Feng, Z. Cheng, Y. Yan, Y. Xu, Y. Jiang, Y. Chang, Y. Lv and P. Lu, Triphenylene-Based Emitters with Hybridized Local and Charge-Transfer Characteristics for Efficient Nondoped Blue OLEDs, *ACS Appl. Mater. Interfaces*, 2023, **15**, 47307–47316.

39 M. F. S. Khan, M. Akbar and J. Wu, Fluorescence and Photophysical Properties of Anthracene and Phenanthrene in Water, *J. Fluoresc.*, 2024, DOI: **10.1007/s10895-024-03905-4**.

40 M. Ikeda, M. Takeuchi and S. Shinkai, Unusual Emission Properties of a Triphenylene-Based Organogel System, *Chem. Commun.*, 2003, **3**, 1354–1355.

41 R. Nandy and S. Sankararaman, Unusual Fluorescence Emission from Ethynyltriphenylene-Substituted Diacetylenic Molecular Hinge, *Org. Biomol. Chem.*, 2010, **8**, 2260–2266.

42 S. Hirata, Recent Advances in Materials with Room-Temperature Phosphorescence: Photophysics for Triplet Exciton Stabilization, *Adv. Opt. Mater.*, 2017, **5**, 1700116.

43 A. Lázaro, C. Cunha, R. Bosque, J. Pina, J. S. Ward, K. N. Truong, K. Rissanen, J. C. Lima, M. Crespo, J. S. Seixas de Melo and L. Rodríguez, Room-Temperature Phosphorescence and Efficient Singlet Oxygen Production, *Inorg. Chem.*, 2020, **59**, 8220–8230.

44 G. M. Sheldrick, A Short History of ShelX, *Acta Crystallogr., Sect. A: Found. Adv.*, 2015, **71**, 3–8.

45 O. V. Dolomanov, L. J. Bourhis, R. J. Gildea, J. A. K. Howard and H. Puschmann, *J. Appl. Crystallogr.*, 2009, **42**, 339–341.

46 G. M. Sheldrick, Crystal Structure Refinement, *Acta Crystallogr., Sect. C: Struct. Chem.*, 2015, **71**, 3–8.

47 (*a*) A. D. Becke, Density-functional exchange-energy approximation with correct asymptotic behavior, *Phys. Rev. A*, 1988, **38**, 3098–3100; (*b*) J. P. Perdew, Density-functional approximation for the correlation energy of the inhomogeneous electron gas, *Phys. Rev. B:Condens. Matter Mater. Phys.*, 1986, **33**, 8822–8824; (*c*) F. Weigend, Accurate Coulomb-Fitting Basis Sets for H to Rn, *Phys. Chem. Chem. Phys.*, 2006, **8**, 1057–1065; (*d*) E. Caldeweyher, S. Ehlert, A. Hansen, H. Neugebauer, S. Spicher, C. Bannwarth and S. A. Grimme, Generally Applicable Atomic-Charge Dependent London Dispersion Correction, *J. Chem. Phys.*, 2019, **150**, 154122.

48 R. Ahlrichs, M. Bär, M. Häser, H. Horn and C. Kölmel, Electronic Structure Calculations on Workstation Computers: The Program System Turbomole, *Chem. Phys. Lett.*, 1989, **162**, 165–169.

49 A. Klampt, WIREs, *Comput. Mol. Sci.*, 2011, **1**, 699–709.

50 T. Yanai, D. Tew and N. Handy, A new hybrid exchange-correlation functional using the Coulomb-attenuating method, *Chem. Phys. Lett.*, 2004, **393**, 51–57.

51 F. Neese, F. Wennmohs, U. Becker and C. Riplinger, *J. Chem. Phys.*, 2020, **152**, 224108.

52 M. Cossi, N. Rega, G. Scalmani and V. Barone, Energies, structures, and electronic properties of molecules in solution with the C-PCM solvation model, *J. Comput. Chem.*, 2003, **24**, 669–681.

53 D. Andrae, U. Haeussermann, M. Dolg, H. Stoll and H. Preuss, *Theor. Chim. Acta*, 1990, **77**, 123–141.